


Hybrid functional pseudopotentials

Jing Yang, Liang Z. Tan, and Andrew M. Rappe*

Department of Chemistry, University of Pennsylvania, Philadelphia, Pennsylvania 19104-6323, USA (Received 11 July 2017; revised manuscript received 30 December 2017; published 16 February 2018)

The consistency between the exchange-correlation functional used in pseudopotential construction and in the actual density functional theory calculation is essential for the accurate prediction of fundamental properties of materials. However, routine hybrid density functional calculations at present still rely on generalized gradient approximation pseudopotentials due to the lack of hybrid functional pseudopotentials. Here, we present a scheme for generating hybrid functional pseudopotentials, and we analyze the importance of pseudopotential density functional consistency for hybrid functionals. For the PBE0 hybrid functional, we benchmark our pseudopotentials for structural parameters and fundamental electronic gaps of the Gaussian-2 (G2) molecular dataset and some simple solids. Our results show that using our PBE0 pseudopotentials in PBE0 calculations improves agreement with respect to all-electron calculations.

DOI: [10.1103/PhysRevB.97.085130](https://doi.org/10.1103/PhysRevB.97.085130)

I. INTRODUCTION

Density functional theory (DFT) methods have proven to be successful for understanding and predicting the physical and chemical properties of materials. With approximations such as the local density approximation (LDA) [1] and the generalized-gradient approximation (GGA) [2], DFT can reproduce many fundamental properties of solids, such as lattice constants and atomization energies [3]. However, the LDA and the GGA usually underestimate the fundamental band gaps of semiconductors and insulators [4]. The use of hybrid functionals in DFT, which combine part of the exact Hartree-Fock (HF) exchange with local or semilocal approximations (PBE0, HSE, B3LYP) [5–7], has become a popular option for addressing this problem.

The pseudopotential approximation is often used to reduce the complexity of DFT calculations. By replacing the nucleus and core electrons with a finite shallow potential, the solution of the Kohn-Sham equation is simplified because of the reduced number of electrons in the system. Accuracy is preserved because the core electrons are not involved in chemical bonding [8,9].

Even though hybrid density functional calculations using pseudopotentials are currently very popular, these calculations solve the Kohn-Sham equation using pseudopotentials constructed at a lower rung of Jacob's ladder [10], such as the GGA. This is due to a lack of hybrid functional pseudopotentials available to the community. The mismatch of the level of the density functional approximation between pseudopotential construction and target calculation is theoretically unjustified, and could lead to reduced accuracy [11]. In this work, we have developed hybrid density functional pseudopotentials to restore pseudopotential consistency in hybrid functional DFT calculations.

Prior to this work, Hartree-Fock pseudopotentials developed over the past decade [12,13] have proven to be useful in calculations with correlated electrons. The inclusion of HF exchange leads to stronger electron binding and mitigates the underbinding errors of the GGA. It has been suggested that HF pseudopotentials may be useful in a variety of contexts, such as modeling systems with negatively charged reference states [13] and in diffusion Monte Carlo simulations [14,15]. The successful development of HF pseudopotentials [13] has opened the possibility of constructing hybrid pseudopotentials by including an exact exchange component into GGA potentials. Previous work demonstrated PBE0 pseudopotentials for gallium, indium, and nitrogen atoms [16]. However, such pseudopotentials were simple linear combinations of the HF pseudopotential and the GGA pseudopotential without self-consistently solving hybrid PBE0 all-electron calculations.

In this paper, we construct consistent pseudopotentials (Sec. II) for the PBE0 hybrid density functional, following the Rappe-Rabe-Kaxiras-Joannopoulos (RRKJ) method [8]. This work extends Ref. [13], which was solely concerned with HF pseudopotentials, by considering self-consistent solutions of a pseudoatom under PBE0, thus moving beyond the non-self-consistent scheme of Ref. [16]. We benchmark the hybrid functional pseudopotential accuracy for diatomic molecules in the G2 dataset and for simple solids, focusing on geometric parameters and band gaps (Sec. III). We find that the use of consistent PBE0 pseudopotentials improves the accuracy of PBE0 calculations of molecules and solids. Using these pseudopotentials, the mean absolute relative error (MARE) of highest occupied molecular orbital–lowest unoccupied molecular orbital (HOMO-LUMO) gaps of molecules is reduced to 4.5% from the MARE of 7.96% obtained by inconsistently using PBE pseudopotentials in PBE0 calculations. Likewise, the MARE of band gaps of simple solids is reduced to 6.56% from 7.90%. The use of consistent PBE0 pseudopotentials was found to have a relatively small effect on bond lengths (MARE reduced to 0.53% from 0.71%) and lattice parameters (MARE reduced to 0.57% from 0.66%). The mean absolute

*rappe@sas.upenn.edu

errors (MAEs), which illustrate the absolute deviation of using pseudopotentials from all-electron PBE0 calculations, indicates the same performance. The PBE0 pseudopotential generator is implemented in the OPIUM software package [17].

II. THEORETICAL METHODS

In this section, we provide an overview of the standard theory behind pseudopotential construction before discussing the special considerations that must be taken into account for hybrid functional pseudopotentials.

A. Pseudopotential construction

The all-electron (AE) wave functions and eigenvalues of an atom are the foundation for the construction of all pseudopotentials. The AE Kohn-Sham (KS) equation is

$$\begin{aligned} \left[-\frac{1}{2}\nabla^2 + V_{\text{ion}}(\mathbf{r}) + V_{\text{H}}[\rho(\mathbf{r})] + V_{\text{xc}}[\rho(\mathbf{r})]\right]\psi_i^{\text{AE}}(\mathbf{r}) \\ = \epsilon_i^{\text{AE}}\psi_i^{\text{AE}}(\mathbf{r}), \end{aligned} \quad (1)$$

where $-\frac{1}{2}\nabla^2$ is the single-particle kinetic-energy operator, $V_{\text{ion}}(\mathbf{r})$ is the ionic potential that electrons feel from the nucleus, $V_{\text{H}}[\rho(\mathbf{r})]$ is the Hartree potential, and $V_{\text{xc}}[\rho(\mathbf{r})]$ is the exchange-correlation potential, which are functionals of the charge density $\rho(\mathbf{r})$. The all-electron wave function is denoted by $\psi_i^{\text{AE}}(\mathbf{r})$, and the all-electron energy eigenvalues are denoted by ϵ_i^{AE} . For an atom, $V_{\text{ion}}(\mathbf{r}) = -\frac{Z}{r}$, where Z is the nuclear charge. Representing the wave function in spherical coordinates, $r = |\mathbf{r}|$, and each $\psi_i^{\text{AE}}(\mathbf{r})$ can be written as

$$\psi_{nlm}^{\text{AE}}(\mathbf{r}) = \frac{\phi_{nl}^{\text{AE}}(r)}{r} Y_{lm}(\theta, \phi), \quad (2)$$

where n, l, m are principal, angular, and spin quantum numbers, and θ and ϕ are the corresponding angles from spherical coordinates. ϕ_{nl}^{AE} is the radial wave function and $Y_{lm}(\theta, \phi)$ are the spherical harmonics. Now, Eq. (1) can be simplified in terms of ϕ_{nl} :

$$\left(-\frac{1}{2}\frac{d^2}{dr^2} + \frac{l(l+1)}{r^2} + V_{\text{KS}}(r)\right)\phi_{nl}^{\text{AE}}(r) = \epsilon_{nl}^{\text{AE}}\phi_{nl}^{\text{AE}}(r), \quad (3)$$

where $V_{\text{KS}}(r) = V_{\text{ion}}(r) + V_{\text{H}}(r) + V_{\text{xc}}(r)$. Instead of solving the full all-electron KS equation as in [Eq. (1)], it is computationally more efficient to solve the radial equation [Eq. (3)] self-consistently to obtain the radial wave function, $\phi_{nl}^{\text{AE}}(r)$, and corresponding eigenvalue, $\epsilon_{nl}^{\text{AE}}$.

In most molecular or solid systems, the valence electrons of atoms within the system are more crucial than core electrons, because they are more involved in chemical bonding. The core electrons mostly contribute to the electrostatic shielding of the nucleus. The AE wave functions of core electrons can contain rapid oscillations, which makes them hard to represent in plane-wave basis sets and causes further difficulty in solving Eq. (3) numerically. Therefore, it is advantageous to construct pseudopotentials, which capture the valence electron behavior and also eliminate the need to recalculate the core-electron wave functions.

Replacing the potential by a pseudopotential operator, the KS equation can be written as

$$\left[-\frac{1}{2}\frac{d^2}{dr^2} + \frac{l(l+1)}{2r^2} + \hat{V}_{\text{PS}}\right]\phi_{nl}^{\text{PS}}(r) = \epsilon_{nl}^{\text{PS}}\phi_{nl}^{\text{PS}}(r), \quad (4)$$

where \hat{V}_{PS} is the screened pseudopotential operator. Note that such an operator is usually nonlocal [it is an integral operator on $\phi_{nl}^{\text{PS}}(r)$]. Similar to V_{KS} , $\hat{V}_{\text{PS}} = \hat{V}_{\text{ion}}^{\text{PS}} + V_{\text{H}}(r) + V_{\text{xc}}(r)$. $\epsilon_{nl}^{\text{PS}}$ is the pseudoeigenvalue, and $\phi_{nl}^{\text{PS}}(r)$ is the pseudo-wave-function. Standard methods for constructing these quantities are given in Appendix A.

B. Hartree-Fock pseudopotentials

Pseudopotentials can be constructed by solving the all-electron (AE) and pseudopotential (PSP) equations, Eqs. (1) and (4), above using different exchange-correlation functionals, such as the LDA or the GGA. It is crucial that the exchange-correlation functional used for pseudopotential construction is the same as the functional used in the target calculation [11]. When the exchange-correlation functional contains the Fock operator, as is the case for the hybrid functionals presently in widespread use, there are special considerations that must be taken into account in constructing the pseudopotential. Here, we consider the case of Hartree-Fock (HF) pseudopotentials, where the exchange-correlation functional is just the Fock operator, and we will examine the PBE0 hybrid functional in the next subsection, where the Fock operator and PBE exchange correlation are combined. For the HF pseudopotential, instead of solving the KS equation as in Eq. (3), we solve the Hartree-Fock equation,

$$(\hat{T} + V_{\text{ion}}(\mathbf{r}) + \hat{V}_{\text{HF}}[\{\psi_{n'l'}\}])\psi_{nl}(\mathbf{r}) = \epsilon_{nl}\psi_{nl}(\mathbf{r}), \quad (5)$$

where $\psi_{nl}(\mathbf{r})$ still takes the form in Eq. (2) (dropping the AE superscript for simplicity), $V_{\text{ion}}(\mathbf{r})$ is the ionic potential, and $\hat{V}_{\text{HF}}[\{\psi_{nl}\}]$ is the HF potential, which depends on the set of wave functions $\{\psi_{nl}\}$. It is separated into two terms,

$$\hat{V}_{\text{HF}}[\{\psi_{n'l'}\}] = \hat{V}_{\text{H}}[\{\psi_{n'l'}\}] + \hat{V}_{\text{x}}[\{\psi_{n'l'}\}]. \quad (6)$$

The Hartree potential takes the form

$$\langle\psi_{nl}|\hat{V}_{\text{H}}[\{\psi_{n'l'}\}]|\psi_{nl}\rangle = \sum_{n'l'} \int d^3\mathbf{r}' d^3\mathbf{r} \frac{|\psi_{n'l'}(\mathbf{r}')|^2 |\psi_{nl}(\mathbf{r})|^2}{|\mathbf{r} - \mathbf{r}'|}, \quad (7)$$

and the exact exchange operator acts as

$$\begin{aligned} \langle\psi_{nl}|\hat{V}_{\text{x}}[\{\psi_{n'l'}\}]|\psi_{nl}\rangle \\ = \sum_{n'l'} \int d^3\mathbf{r}' d^3\mathbf{r} \frac{\psi_{nl}(\mathbf{r})\psi_{n'l'}^*(\mathbf{r})\psi_{n'l'}(\mathbf{r}')\psi_{nl}^*(\mathbf{r}')}{|\mathbf{r} - \mathbf{r}'|}. \end{aligned} \quad (8)$$

Direct evaluation of the Fock integral above [Eq. (8)] requires introduction of angular variables for orbitals with nonzero angular momentum. This would result in nonspherical pseudopotentials, as well as introducing complexity into the pseudopotential generation process, which would then depend on the exact atomic configuration, including magnetic quantum numbers. To circumvent these issues, we make use of a spherical approximation to construct spherical Hartree-Fock pseudopotentials. Spherical approximations are routinely used to construct spherical LDA and GGA pseudopotentials, which

are widely used successfully in electronic and structural calculations.

We use the Hartree-Fock spherical approximation of Froese Fischer [18] based on the concept of the ‘‘average energy of configuration’’ introduced by Slater [19]. Consider all atomic configurations where the i th shell, with principal and total angular quantum numbers n_i and l_i , is occupied with weight w_i , that is, all permutations of w_i electrons occupying the $(2l_i + 1)$ -degenerate shell ($n_i l_i$).

The average energy of all such atomic configurations, expressed as a sum over pairs of atomic orbitals ($n_i l_i$) and ($n_j l_j$), is

$$E_{\text{av}}^{\text{HF}} = \sum_{i=1}^m w_i \left[I(n_i l_i, n_i l_i) + \left(\frac{w_i - 1}{2} \right) \times \sum_{k=0}^{2l_i} f_k(l_i, l_i) F^k(n_i l_i, n_i l_i) \right] + \sum_{i=2}^m \left\{ \sum_{j=1}^{i-1} w_i w_j \left[F^0(n_i l_i, n_j l_j) + \sum_{k=|l_i-l_j|}^{(l_i+l_j)} g_k(l_i, l_j) G^k(n_i l_i, n_j l_j) \right] \right\}. \quad (9)$$

Here, the first summation represents the one-electron contribution,

$$I(nl, nl) = -\frac{1}{2} \int_0^\infty \phi_{nl}^*(r) \left(\frac{d^2}{dr^2} + \frac{2Z}{r} - \frac{l(l+1)}{r^2} \right) \phi_{nl}(r) dr. \quad (10)$$

The other terms contain the interaction terms between pairs of electrons. F^k and G^k are the Hartree and exchange energy Slater integrals,

$$F^k(nl; n'l') = \int_0^\infty \int_0^\infty \phi_{nl}(r) \phi_{nl}(r) \frac{r_{<}^k}{r_{>}^{k+1}} \phi_{n'l'}(r') \phi_{n'l'}(r') dr dr' \quad (11)$$

and

$$G^k(nl; n'l') = \int_0^\infty \int_0^\infty \phi_{nl}(r) \phi_{n'l'}(r') \times \frac{r_{<}^k}{r_{>}^{k+1}} \phi_{n'l'}(r) \phi_{nl}(r') dr dr', \quad (12)$$

where $r_{<}$ ($r_{>}$) is the lesser (greater) of r and r' . Details of the derivation are provided in Appendix C, and the numerical coefficients f_k and g_k are tabulated in Ref. [19]. We note that the integrals in Eqs. (10)–(12) for the average energy depend only on the radial coordinate, and hence are a simplification of Eqs. (7) and (8).

Taking functional derivatives of Eq. (9) with respect to the radial wave functions $\phi_i(r)$, we arrive at Hartree-Fock equations for the wave functions of a Hartree-Fock atom. The set of m radial wave functions ϕ_i , $i = 1, \dots, m$, obeys the coupled set of equations

$$\hat{L} \phi_i(r) = \frac{2}{r} [Y_i[\{\phi\}](r) \phi_i(r) + X_i[\{\phi\}](r)] + \sum_{j=1}^m \varepsilon_{ij} \phi_j(r), \quad (13)$$

where $\hat{L} = \frac{d^2}{dr^2} - 2V_{\text{ion}}(r) - \frac{l_i(l_i+1)}{r^2}$ is the single-particle part of the Hartree-Fock Hamiltonian, $(2/r)Y_i[\{\phi\}](r)$ and $(2/r)X_i[\{\phi\}](r)$ are the Hartree and exchange terms [20], and ε_{ij} are Lagrange multipliers for orthogonality and normalization of radial wave functions. The detailed derivations of all these terms are presented in Appendix C.

Once the HF equation is constructed, we solve these equations self-consistently in a similar way to DFT pseudopotentials. The HF pseudo-wave-functions $\phi_{nl}^{\text{PS}}(r)$ are constructed using the same RKKJ procedure [Eq. (A1)] as for the DFT pseudo-wave-functions. The screened pseudopotential is obtained by inverting Eq. (5). Similar to DFT pseudopotentials, we descreen by subtracting the Hartree and exchange contributions of the valence electrons [cf. Eq. (A2)],

$$V_{\text{ion},l}^{\text{PS}}(r) = V_l^{\text{PS}}(r) - \frac{2}{r} Y_i[\{\phi_{\text{val}}\}](r) - \frac{2X_i[\{\phi_{\text{val}}\}](r)}{r\phi_i(r)}, \quad (14)$$

with Y_i and X_i obtained from Eq. (13). The HF pseudopotential constructed this way has a long-range non-Coulombic component of the tail, which does not decay as $1/r$. This is a consequence of the nonlocal nature of the Fock operator [13]. To resolve this issue, we make use of the localization procedure of Trail and Needs [12]. The tail is forced to asymptotically approach $1/r$, and the potential is modified within the localization radius to ensure consistency with the all-electron eigenvalues [13].

C. PBE0 pseudopotentials

As hybrid functionals are a mix of HF and DFT ingredients, we generate a hybrid pseudopotential using the HF pseudopotential approach as a foundation, making use of the spherical averaging procedure and localization procedure of the previous section and Ref. [13]. The PBE0 density functional [21] was developed based on the PBE exchange-correlation functional [2]; the PBE0 form is

$$E_{\text{xc}}^{\text{PBE0}} = aE_{\text{x}}^{\text{HF}} + (1-a)E_{\text{x}}^{\text{PBE}} + E_{\text{c}}^{\text{PBE}}, \quad (15)$$

where $a = 0.25$ for the PBE0 functional. As we use the spherical approximation for E_{x}^{HF} [Eq. (9)], we likewise evaluate the PBE exchange-correlation functional using a spherical approximation. Since $E_{\text{x}}^{\text{PBE}}$ is a functional of density only, this method consists of evaluating $E_{\text{x}}^{\text{PBE}}$ in Eq. (15) at the charge density, again taken to be the average over all possible magnetic quantum number configurations,

$$\rho(r) = \sum_{nlm} f_{nlm} |\psi(\mathbf{r})_{nl}|^2 = \frac{1}{4\pi} \sum_{n_i l_i} f_{n_i l_i} |\phi_{n_i l_i}(r)|^2, \quad (16)$$

where $\rho(r)$ is the spherical symmetric charge density, $f_{n_i l_i} = w_i$ (as in Appendix B) is the occupation number for each orbital ($n_i l_i$), and $f_{nlm} = f_{nlm'}$ is the occupation number for each magnetic quantum number (nlm). Upon including $E_{\text{x}}^{\text{PBE}}$ and $E_{\text{c}}^{\text{PBE}}$ into the total energy expression Eq. (9), and taking functional derivatives, the coupled set of HF equations

[Eq. (13)] becomes

$$\hat{L}\phi_i(r) = \frac{2}{r} \left[Y_i(r)\phi_i(r) + \frac{1}{4}X_i(r) \right] + \frac{3}{4}V_x^{\text{PBE}}(r) + V_c^{\text{PBE}}(r) + \sum_{j=1}^m \delta_{l_i, l_j} \epsilon_{ij} \phi_j(r), \quad (17)$$

where the additional terms are the PBE exchange potential $V_x^{\text{PBE}}(r)$ and the PBE correlation potential $V_c(r)$. The self-consistent solution of these coupled equations is found iteratively, in a similar fashion to the HF equations [Eq. (13)]. At each iteration, we calculate the Fock exchange term $[X_i(r)]$ from the wave functions of the previous iteration, and the PBE terms (V_x^{PBE} , V_c^{PBE}) from the density of the previous iteration. The pseudopotential construction is performed in the same way as for HF pseudopotentials, including RRKJ pseudization, descreening, and localization of the non-Coulombic tail.

III. TESTING OF PBE0 PSEUDOPOTENTIALS ON MOLECULAR AND SOLID-STATE SYSTEMS

We test the accuracy of our PBE0 pseudopotentials and the importance of pseudopotential density functional consistency for PBE0. We compare PBE calculations using PBE pseudopotentials (PBE), PBE0 calculations using PBE0 pseudopotentials (PBE0), and PBE0 calculations using PBE pseudopotentials (PBE-PBE0). The last case is currently the most widely used method of performing PBE0 calculations. The DFT code we use is QUANTUM-ESPRESSO [22]. Each single molecule is put into a 20.0 Å cubic unit cell, and its energy and geometry are computed with a kinetic energy cutoff $E_{\text{cut}} = 25.0$ Hartree. All these calculations are spin-polarized. The total energy convergence threshold and force convergence threshold are set to 0.005 mHartree/cell and 0.05 mHartree/Å. The reference all-electron calculations are performed using FHI-aims [23] with tight basis settings. The molecular and crystal structural optimizations are converged within 3×10^{-3} mHartree/cell for total energy, and the forces are converged within 0.003 mHartree/Å.

In Table I, we show the bond lengths for diatomic molecules that belong to the G2 data set [5], and we compare each of our pseudopotential calculations with PBE0 all-electron values [24]. The use of the PBE pseudopotential in the PBE0 calculation gives a MARE of 0.71%. Using the PBE0 functional with the PBE0 pseudopotential, the MARE reduces to 0.53%. This indicates that pseudopotential density functional consistency improves bond lengths for PBE0.

One of the reasons for using hybrid density functionals is that they predict band structures and ionization potentials (IPs) more accurately than the PBE functional [16,25,26]. Table II shows the HOMO eigenvalues for diatomic molecules within the G2 dataset, calculated from different density functionals and compared with HOMO levels calculated from all-electron calculations. As expected, the difference between PBE HOMO eigenvalues and all-electron PBE0 values is the largest among the three computed cases. The use of consistent PBE0 pseudopotentials improves the MARE of the HOMO eigenvalues by a small amount [to 6.66% (PBE0) from 6.79% (PBE-PBE0)].

TABLE I. The bond lengths of the diatomic molecules from the G2 data set calculated from PBE, PBE-PBE0, and PBE0. The all-electron data are calculated using FHI-aims [23]. Units in Å. The MARE is calculated as $\text{MARE} = \frac{1}{N} \sum_i^N \frac{|b_i - b_{\text{AE}}|}{b_{\text{AE}}} \times 100$, where N is the number of species, b_i is the bond length of each species, and b_{AE} is the all-electron value. The MAE is the average absolute deviation over the presented molecules and is calculated as $\text{MAE} = \frac{1}{N} \sum_i^N |b_i - b_{\text{AE}}|$. MARE and MAE of PBE calculations are taken relative to AE-PBE, while that of PBE0 calculations are taken relative to AE-PBE0. The experimental values are also listed for reference. The rest of the tables are of the same format.

Molecule	PBE	AE-PBE	PBE-PBE0	PBE0	AE-PBE0	Expt. ^a
H ₂	0.753	0.750	0.747	0.747	0.746	0.742
LiH	1.600	1.603	1.595	1.596	1.595	1.595
BeH	1.348	1.355	1.343	1.351	1.348	1.343
CH	1.137	1.136	1.122	1.122	1.124	1.120
NH	1.070	1.050	1.056	1.041	1.041	1.045
OH	0.983	0.983	0.975	0.966	0.983	0.971
FH	0.928	0.93	0.914	0.912	0.918	0.917
Li ₂	2.719	2.728	2.725	2.718	2.723	2.670
LiF	1.578	1.574	1.567	1.566	1.562	1.564
CN	1.174	1.175	1.159	1.159	1.159	1.172
CO	1.135	1.136	1.123	1.122	1.122	1.128
N ₂	1.081	1.103	1.069	1.069	1.089	1.098
NO	1.132	1.157	1.113	1.138	1.139	1.151
O ₂	1.212	1.218	1.218	1.217	1.192	1.207
F ₂	1.420	1.413	1.382	1.382	1.376	1.412
MARE (%)	0.61		0.71	0.53		
MAE (Å)	0.007		0.008	0.006		

^aReference [24].

In Table III, we present the HOMO-LUMO gap for the same dataset as in Table II. Our PBE0 pseudopotentials reduce the MARE of the HOMO-LUMO gap to 4.55% (PBE0) from 7.96% (PBE-PBE0). Similar to bond length calculations, the

TABLE II. HOMO eigenvalues with PBE, PBE-PBE0, and PBE0 methods. Energies are in eV.

Molecule	PBE	AE-PBE	PBE-PBE0	PBE0	AE-PBE0
H ₂	-10.31	-10.34	-11.96	-11.96	-11.99
LiH	-3.89	-4.35	-5.45	-5.44	-5.44
BeH	-4.76	-4.68	-5.77	-5.20	-5.69
CH	-5.91	-5.84	-7.43	-7.43	-7.45
NH	-7.98	-6.69	-9.78	-9.76	-9.76
OH	-7.06	-7.14	-8.81	-8.72	-7.00
FH	-9.33	-9.61	-11.43	-11.43	-11.86
Li ₂	-3.20	-3.16	-3.99	-3.75	-3.72
LiF	-6.08	-6.09	-7.77	-7.85	-7.96
CN	-9.30	-9.38	-10.74	-10.94	-9.32
CO	-9.01	-9.03	-10.41	-10.42	-10.72
N ₂	-10.07	-10.22	-11.93	-12.20	-12.20
NO	-4.74	-4.50	-6.25	-6.29	-4.60
O ₂	-6.71	-6.91	-8.68	-8.70	-8.91
F ₂	-9.41	-9.46	-11.50	-11.58	-11.68
MARE (%)	3.33		6.79	6.66	
MAE (eV)	3.15		0.40	0.38	

TABLE III. HOMO-LUMO gap (in eV) of diatomic molecules in the G2 dataset with different functionals.

Molecule	PBE	AE-PBE	PBE-PBE0	PBE0	AE-PBE0	Expt.
H ₂	10.26	10.84	11.94	11.94	13.10	11.8 ^a
LiH	2.57	2.81	4.04	4.48	4.45	4.0410 ^b
BeH	2.64	2.31	4.44	4.42	4.15	4.200 ^b
CH	2.06	1.77	3.95	3.51	3.60	
NH	3.95	6.45	7.27	7.34	7.16	
OH	1.12	6.54	4.77	4.92	4.25	
FH	8.19	8.76	10.92	10.93	11.80	11.30 ^a
Li ₂	1.41	1.43	2.75	2.47	2.50	2.22 ^b
LiF	4.29	4.62	6.41	6.50	7.02	6.16 ^b
CN	1.99	1.72	4.67	4.74	4.48	9.78 ^b
CO	6.98	6.98	9.61	9.62	10.04	10.29 ^b
N ₂	7.66	8.24	10.94	10.94	11.71	11.05 ^b
NO	1.30	1.22	3.50	2.88	2.86	3.05 ^b
O ₂	2.40	2.31	5.74	6.09	6.10	6.06 ^c
F ₂	3.32	3.63	7.77	7.79	8.34	7.47 ^b
MARE (%)	14.82		7.96	4.55		
MAE (eV)	0.78		0.50	0.39		

^aReference [27].^bReference [28], G4 basis set.^cReference [29].

consistency of the density functional between pseudopotential construction and DFT calculation reduces the error. While the use of the PBE pseudopotential for PBE0 DFT calculation results in fair accuracy, it can be improved by using a pseudopotential constructed with a consistent density functional.

We have also tested our pseudopotentials in solid-state calculations. The lattice constants and band gaps for some simple solids associated with the first 20 elements in the Periodic Table are shown in Tables IV and V. Similar to molecular bond lengths, the density functional consistency also influences the lattice constants of solids. By using consistent pseudopotentials, the MARE of lattice constants of these solids are slightly improved to 0.57% (PBE0) from 0.66% (PBE-PBE0). As expected, the PBE calculation significantly underestimates the band gaps. The two PBE0 cases increase

TABLE IV. Solid-state calculation with PBE, PBE-PBE0, and PBE0. The lattice constants of simple solids associated with the first 20 elements are listed. The lattice constant is in units of Å.

Solids	PBE	AE-PBE	PBEPBE0	PBE0	AE-PBE0	Expt. ^a
Si	5.484	5.472	5.452	5.446	5.448	5.430
GaN	4.541	4.549	4.539	4.537	4.536	4.523
MgO	4.324	4.305	4.310	4.308	4.204	4.207
NaCl	5.710	5.701	5.663	5.639	5.634	5.595 ^b
Diamond	3.562	3.563	3.562	3.563	3.564	3.567
Graphene	2.476	2.469	2.460	2.460	2.453	2.464 ^c
BN (cubic)	3.664	3.665	3.639	3.639	3.598	3.616
SiC	4.403	4.404	4.375	4.370	4.349	4.358
MARE (%)	0.17		0.66	0.57		
MAE (Å)	0.007		0.027	0.023		

^aReference [7].^bReference [26].^cReference [30].

TABLE V. Solid-state calculation with PBE, PBE-PBE0, and PBE0. The band gap of simple solids within the first 20 elements are listed. The band gap is in eV.

Solids	PBE	AE-PBE	PBEPBE0	PBE0	AE-PBE0	Expt. ^a
Si	0.58	2.54	1.79	1.78	1.63	1.17
GaN	1.81	1.55	3.58	3.56	3.54	3.30
MgO	4.38	4.44	7.97	7.38	7.28	7.22
NaCl	3.67	4.97	6.71	7.28	7.14	8.50 ^b
Diamond	5.63	5.58	5.53	5.54	6.08	5.48
BN (cubic)	4.49	4.45	6.58	6.56	6.54	6.22
SiC	1.34	1.38	2.98	2.96	2.95	2.42
MARE (%)	18.02		5.29	3.78		
MAE (eV)	0.53		0.28	0.18		

^aReference [7].^bReference [26].

the band gaps by a large amount compared to PBE calculation. The effect of density functional consistency is even more important for the band gaps than for the lattice constants: the MAREs of the band gaps are improved to 3.78% (PBE0) from 5.29% (PBE-PBE0). Together with the calculations from molecular properties, we may conclude that pseudopotential density functional inconsistency contributes a systematic error of the order of 1% for PBE0 for the systems tested.

IV. CONCLUSION

We have developed a consistent PBE0 pseudopotential and successfully implemented it in the OPIUM pseudopotential generation code. We have also shown that our PBE0 pseudopotentials behave well when implementing them in DFT calculations. Our benchmarking tests on the G2 dataset and solids indicate that the systematic error associated with pseudopotential density functional consistency is of the order of 1%. Using the PBE0 pseudopotential in PBE0 DFT calculations leads to small improvements in bond length and lattice parameter accuracy. For these quantities, the errors of the pseudopotential calculations compared to all-electron calculations are typically less than 1%. Using consistent PBE0 pseudopotentials reduces these errors by around 0.1% (i.e., pseudopotential density functional consistency accounts for about 1/10th of the 1% errors in these geometrical quantities). On the other hand, for the HOMO-LUMO gaps, the error of the pseudopotential calculations compared to all-electron calculations is 8%, and is reduced to 4.5% by using PBE0 pseudopotentials. Pseudopotential density functional consistency, therefore, accounts for a significant amount of the error between pseudopotential and all-electron calculations, for the electronic excitation energies. A similar trend is obtained for the band gaps of solids tested. From these results, we conclude that using PBE pseudopotentials in PBE0 calculations leads to acceptable results for small molecules and simple solids, while using PBE0 pseudopotentials instead will likely result in a small but consistent increase in accuracy. Future directions include further testing of PBE0 pseudopotentials for more complex systems, the inclusion of relativistic effects for heavy atoms, and the development of other hybrid functional pseudopotentials, including range-separated hybrids [31].

ACKNOWLEDGMENTS

J.Y. was supported by the U.S. National Science Foundation, under Grant No. DMR-1719353. L.Z.T. was supported by the U.S. ONR under Grant No. N00014-17-1-2574. A.M.R. was supported by the U.S. Department of Energy under Grant No. DE-FG02-07ER46431. Computational support was provided by the High Performance Computing Modernization Program of the Department of Defense and the National Energy Research Scientific Computing Center of the Department of Energy.

APPENDIX A: DETAILS OF PSEUDOPOTENTIAL CONSTRUCTION

Norm-conserving pseudo-wave-functions [32] should obey the following criteria:

- (i) $\phi_{nl}^{\text{PS}}(r) = \phi_{nl}^{\text{AE}}(r)$, $\frac{d\phi_{nl}^{\text{PS}}(r)}{dr} = \frac{d\phi_{nl}^{\text{AE}}(r)}{dr}$,
 $\frac{d^2\phi_{nl}^{\text{PS}}(r)}{dr^2} = \frac{d^2\phi_{nl}^{\text{AE}}(r)}{dr^2}$ for $r \geq r_c$,
- (ii) $\epsilon_{nl}^{\text{PS}} = \epsilon_{nl}^{\text{AE}}$,
- (iii) $\langle \phi_{nl}^{\text{PS}} | \phi_{nl}^{\text{PS}} \rangle = \langle \phi_{nl}^{\text{AE}} | \phi_{nl}^{\text{AE}} \rangle = 1$,
- (iv) $\left. \frac{d}{d\epsilon} \left(\frac{d \ln \phi_{nl}^{\text{PS}}(r)}{dr} \right) \right|_{R, \epsilon_{nl}} = \left. \frac{d}{d\epsilon} \left(\frac{d \ln \phi_{nl}^{\text{AE}}(r)}{dr} \right) \right|_{R, \epsilon_{nl}}$,
 $R \geq r_c$.

Together, they guarantee wave-function smoothness and continuity, that the solutions of the pseudosystem are accurate representations of the corresponding all-electron system, and that the error of eigenenergy shifts caused by chemical bonding is small for gentle changes to the wave functions and density [32], hence improving the transferability or applicability of the pseudopotential in different chemical environments.

In the RRKJ method [8], the pseudo-wave-function is constructed as a sum of N_b spherical Bessel functions $j_l(q_k r)$:

$$\phi_{nl}^{\text{PS}}(r) = \begin{cases} \sum_{k=1}^{N_b} c_{nlk} r j_l(q_k r), & r < r_c, \\ \phi_{nl}^{\text{AE}}(r), & r \geq r_c, \end{cases} \quad (\text{A1})$$

where the coefficients c_{nlk} are chosen to normalize the wave function and satisfy continuity constraints at r_c . Additional c_{nlk} coefficients improve plane-wave convergence. Once the pseudo-wave-function is constructed, the pseudopotential is obtained by inverting the pseudo-KS equation above [see Eq. (4)]. In applications of the pseudopotential in solid-state or molecular calculations, the screening effect of the valence electrons will generally be different from that in the atomic calculation. Therefore, the valence electron screening is removed to obtain a descreened pseudopotential, $V_{\text{ion},l}^{\text{PS}}(r)$, for each angular momentum l , by subtracting Hartree and exchange-correlation potentials from the screened pseudopotential,

$$V_{\text{ion},l}^{\text{PS}}(r) = V_l^{\text{PS}}(r) - V_{\text{H}}[\rho_{\text{val}}](r) - V_{\text{xc}}[\rho_{\text{val}}](r), \quad (\text{A2})$$

where $V_{\text{H}}[\rho_{\text{val}}](r)$ and $V_{\text{xc}}[\rho_{\text{val}}](r)$ are calculated only from the valence charge density. The full pseudopotential, written

in semilocal form, is then

$$\begin{aligned} \hat{V}_{\text{ion}}^{\text{PS}} &= \sum_{lm} V_{\text{ion},l}^{\text{PS}}(r) |Y_{lm}\rangle \langle Y_{lm}| \\ &= V_{\text{loc}}(r) + \sum_l \Delta \hat{V}_l^{\text{SL}}. \end{aligned} \quad (\text{A3})$$

In the second line, the potential is expressed as the sum of a local potential $V_{\text{loc}}(r)$ and semilocal corrections $\Delta \hat{V}_l^{\text{SL}}$, which are projections in the angular coordinates and are local in the radial coordinate. To reduce the memory cost of computation, we write the semilocal pseudopotential in a fully separable nonlocal Kleinman-Bylander [33] form

$$\begin{aligned} \hat{V}^{\text{PS}} &= \hat{V}^{\text{loc}} + \sum_l \Delta \hat{V}_l^{\text{NL}}, \\ \Delta \hat{V}_l^{\text{NL}} &= \frac{\Delta \hat{V}_l^{\text{SL}} |\phi_{nl}^{\text{PS}}\rangle \langle \phi_{nl}^{\text{PS}}| \Delta \hat{V}_l^{\text{SL}}}{\langle \phi_{nl}^{\text{PS}} | \Delta \hat{V}_l^{\text{SL}} | \phi_{nl}^{\text{PS}} \rangle}. \end{aligned} \quad (\text{A4})$$

Writing the pseudopotential in this form ensures that semilocal and nonlocal pseudoatoms have the same eigenvalues and wave functions for the reference configuration. The transferability of such a nonlocal pseudopotential, to configurations other than the reference, can be improved by applying the designed nonlocal strategy, which involves modifying the projectors of Eq. (A4) [9].

We implement pseudopotential construction on a radial grid, with accuracy depending on the radial grid size. The use of a logarithmic grid ensures enough grid points near the core to describe oscillations of the all-electron wave functions in that region while capturing the tail of the wave functions at large distances from the core to sufficient accuracy. The logarithmic grid is defined as

$$r_i = aZ^{-1/3} e^{(i-1)b}, \quad i = 1, \dots, N, \quad (\text{A5})$$

where N is the number of grid points, spanning a sufficiently large real-space range (r_{max}), Z is the core charge, a controls the position of the first grid point, and b determines the grid spacing. We use values of $a = 0.0001$ and $b = 0.013$. The number of grid points N is obtained by setting $r_{\text{max}} = 80$ Bohr.

APPENDIX B: DERIVATION OF HARTREE-FOCK AVERAGE ENERGY

As a preliminary to deriving the average energy formula Eq. (9), we collect several useful quantities. The Hartree potential due to an electron in the state (nlm) is

$$\begin{aligned} V_H^{(nlm)}(\vec{r}) &= \int d^3r' \frac{|\psi_{nlm}(\vec{r}')|^2}{|\vec{r} - \vec{r}'|} \\ &= \int_0^\infty r'^2 dr' d\Omega' \frac{\phi_{nl}(r')^2 |Y_{lm}(\Omega')|^2}{|\vec{r} - \vec{r}'|}. \end{aligned} \quad (\text{B1})$$

Using the expansion,

$$\frac{1}{|\vec{r} - \vec{r}'|} = \sum_{k=0}^{\infty} \sum_{m=-k}^k \frac{4\pi}{2k+1} (-1)^m \frac{r_{\leq}^k}{r_{>}^{k+1}} Y_{k,-m}(\Omega) Y_{k,m}(\Omega'), \quad (\text{B2})$$

where $r_<$ ($r_>$) is the lesser (greater) of r and r' , we write Eq. (B1) as

$$\begin{aligned} V_H^{(nlm)}(\vec{r}) &= \sum_k \int_0^\infty r'^2 dr' \frac{r_{\leq}^k}{r_{>}^{k+1}} \sqrt{\frac{4\pi}{2k+1}} Y_{k,0}^*(\Omega) c^k(l,m,l,m) \phi_{nl}(r')^2 \\ &= \int_0^\infty r'^2 dr' \frac{1}{r_>} \phi_{nl}(r')^2 + \sum_{k=1}^{2l} \int_0^\infty r'^2 dr' \frac{r_{\leq}^k}{r_{>}^{k+1}} \sqrt{\frac{4\pi}{2k+1}} Y_{k,0}^*(\Omega) c^k(l,m,l,m) \phi_{nl}(r')^2. \end{aligned} \quad (\text{B3})$$

Here, we make use of the symbols

$$\begin{aligned} c^k(l,m,l',m') &= \sqrt{\frac{4\pi}{2k+1}} \int Y_{lm}^*(\Omega) Y_{k,m-m'}(\Omega) Y_{l'm'}(\Omega) d\Omega \\ &= (-1)^{-m} \sqrt{2l+1} \sqrt{2l'+1} \begin{pmatrix} l & k & l' \\ 0 & 0 & 0 \end{pmatrix} \begin{pmatrix} l & k & l' \\ -m & m-m' & m' \end{pmatrix} \end{aligned} \quad (\text{B4})$$

for Gaunt's formula, in terms of Wigner 3j-symbols. In the second line of Eq. (B3), we have separated the $k=0$ and $k>0$ components, because the latter vanishes when averaged over m . Therefore, the Hartree energy of a pair of electrons ($ij|ij$), in orbitals (n_i, l_i) and (n_j, l_j) , averaged over the magnetic quantum number m_j of the second electron, is simply

$$\begin{aligned} \langle (ij|ij) \rangle_{m_j} &= \int_0^\infty dr \phi_{n_i l_i}(r)^2 \int_0^\infty dr' \frac{1}{r_>} \phi_{n_j l_j}(r')^2 \\ &= F^0(n_i l_i, n_j l_j). \end{aligned} \quad (\text{B5})$$

The exchange integral for a pair of electrons in orbitals (n_i, l_i) and (n_j, l_j) can be calculated in a similar fashion. Using Eqs. (B2) and (B4), we get

$$\begin{aligned} (ij|ji) &= \int d^3r d^3r' \frac{\psi_{n_i l_i m_i}^*(\vec{r}) \psi_{n_j l_j m_j}(\vec{r}) \psi_{n_j l_j m_j}^*(\vec{r}') \psi_{n_i l_i m_i}(\vec{r}')}{|\vec{r} - \vec{r}'|} \\ &= \sum_{kq} \int Y_{l_i m_i}^*(\Omega) Y_{l_j m_j}(\Omega) Y_{kq}(\Omega) d\Omega \int Y_{l_j m_j}^*(\Omega') Y_{l_i m_i}(\Omega') Y_{kq}(\Omega') d\Omega' \\ &\quad \times \int \frac{r_{\leq}^k}{r_{>}^{k+1}} \frac{4\pi}{2k+1} \phi_{n_i l_i}(r) \phi_{n_j l_j}(r) \phi_{n_j l_j}(r') \phi_{n_i l_i}(r') dr dr' \\ &= \sum_k c^k(l_i, m_i, l_j, m_j)^2 \int \frac{r_{\leq}^k}{r_{>}^{k+1}} \phi_{n_i l_i}(r) \phi_{n_j l_j}(r) \phi_{n_j l_j}(r') \phi_{n_i l_i}(r') dr dr'. \end{aligned} \quad (\text{B6})$$

For the average of the exchange integral over m_j , we get

$$\langle (ij|ji) \rangle_{m_j} = \frac{1}{\sqrt{(2l_i+1)(2l_j+1)}} \sum_k c^k(l_i, 0, l_j, 0) G^k(n_i l_i, n_j l_j). \quad (\text{B7})$$

To calculate the average total energy of an atomic configuration, we must consider the Hartree and exchange energies of all pairs of electrons. First consider the case in which the electrons are in the same orbital ($n_i = n_j$, $l_i = l_j$). In this case, since $G^k(n_i l_i, n_i l_i) = F^k(n_i l_i, n_i l_i)$, we can combine Eqs. (B5), (11), and (B7) to obtain

$$\langle (ij|ij) - (ij|ji) \rangle = \frac{w_i(w_i-1)}{2} \sum_k f_k(l_i, l_i) F^k(n_i l_i, n_i l_i), \quad (\text{B8})$$

where the numerical coefficients $f_k(l_i, l_i)$ are obtained from those in Eqs. (B5) and (B7), and the prefactor $\frac{w_i(w_i-1)}{2}$ is the number of different electron pairs in orbital i .

For the case in which the electrons in the pair are in different orbitals, the sum of Eqs. (B5) and (B7) gives

$$\langle (ij|ij) - (ij|ji) \rangle = w_i w_j \left(F^0(n_i l_i, n_j l_j) + \sum_k g_k(l_i, l_j) G^k(n_i l_i, n_j l_j) \right), \quad (\text{B9})$$

where the coefficients $g_k(l_i, l_j)$ are given by Eq. (B7). Collecting the terms in Eqs. (B8) and (B9) with the single-particle energies results in the expression for the average total energy Eq. (9).

APPENDIX C: DERIVATION OF SELF-CONSISTENT HARTREE-FOCK EQUATIONS

If the orbitals are not necessarily normalized, the average energy (as defined in Sec. II B) derived in Appendix B may be written in the form

$$E_{\text{av}}^{\text{HF}} = \sum_i \frac{w_i I(n_i l_i, n_i l_i)}{\langle n_i l_i | n_i l_i \rangle} + \sum_{i;k} \frac{a_{iik} F^k(n_i l_i, n_i l_i)}{\langle n_i l_i | n_i l_i \rangle \langle n_i l_i | n_i l_i \rangle} + \sum_{i>j;k} \frac{a_{ijk} F^k(n_i l_i, n_j l_j)}{\langle n_i l_i | n_i l_i \rangle \langle n_j l_j | n_j l_j \rangle} + \sum_{i>j;k} \frac{b_{ijk} G^k(n_i l_i, n_j l_j)}{\langle n_i l_i | n_i l_i \rangle \langle n_j l_j | n_j l_j \rangle}. \quad (\text{C1})$$

We wish to find wave functions that minimize $E_{\text{av}}^{\text{HF}}$ under the constraint of wave-function orthogonality. In other words, a pair of radial functions from orbitals with the same angular momentum, (n_i, l_i) and (n_j, l_j) with $l_i = l_j$, must be orthogonal. Using the Lagrange multipliers λ_{ij} , we therefore search for the stationary solutions of the functional

$$K = E_{\text{av}}^{\text{HF}} + \sum_{i>j} \delta_{l_i l_j} \lambda_{ij} \frac{\langle n_i l_i | n_j l_j \rangle}{\langle n_i l_i | n_i l_i \rangle^{1/2} \langle n_i l_i | n_i l_i \rangle^{1/2}}. \quad (\text{C2})$$

We now proceed to take functional derivatives of Eqs. (C1) and (C2) with respect to variations in a radial function $\phi_{nl}(r)$. We note that only a subset of terms in Eq. (C1) involves nl , and those that do all contain a factor of $\langle n_i l_i | n_i l_i \rangle^{-1}$. We can therefore write those terms in the form $\tilde{E}(nl) = \langle n_i l_i | n_i l_i \rangle^{-1} \tilde{F}(nl)$ with the variation

$$\delta \tilde{E}(nl) = \langle n_i l_i | n_i l_i \rangle^{-1} \delta \tilde{F}(nl) + \delta[\langle n_i l_i | n_i l_i \rangle^{-1}] \tilde{F}(nl) \quad (\text{C3})$$

and

$$\begin{aligned} \delta \tilde{F}(nl) = & w_{nl} \delta I(nl) + \sum_k a_{nl,nl,k} F^k(nl, nl) \delta[\langle nl | nl \rangle^{-1}] + \sum_k \frac{a_{nl,nl,k} \delta F^k(nl, nl)}{\langle nl | nl \rangle} + \sum_{n'l' \neq nl, k} \frac{a_{nl,n'l',k} \delta F^k(nl, n'l')}{\langle n'l' | n'l' \rangle} \\ & + \sum_{n'l' \neq nl, k} \frac{b_{nl,n'l',k} \delta G^k(nl, n'l')}{\langle n'l' | n'l' \rangle}. \end{aligned} \quad (\text{C4})$$

Furthermore, we have

$$\delta[\langle n_i l_i | n_i l_i \rangle^{-1}] = -2 \int dr \frac{\phi_{nl}(r) \delta \phi_{nl}(r)}{\langle nl | nl \rangle^2} \quad (\text{C5})$$

and

$$\delta F^k(nl, n'l') = 2(1 + \delta_{nl, n'l'}) \int dr \phi_{nl}(r) \delta \phi_{n'l'}(r) \frac{1}{r} Y^k(n'l', nl, r), \quad (\text{C6})$$

$$\delta G^k(nl, n'l') = 2 \int dr \phi_{n'l'}(r) \delta \phi_{nl}(r) \frac{1}{r} Y^k(nl, n'l', r), \quad (\text{C7})$$

where

$$Y^k(nl, n'l', r) = \int_0^r ds \frac{s^k}{r^k} \phi_{nl}(s) \phi_{n'l'}(s) + \int_r^\infty ds \frac{r^{k+1}}{s^{k+1}} \phi_{nl}(s) \phi_{n'l'}(s). \quad (\text{C8})$$

Finally, the variation of the terms involving the Lagrange multipliers in Eq. (C2) is

$$\delta \left[\sum_{n'} \lambda_{nl, n'l'} \frac{\langle nl | n'l' \rangle}{\langle nl | nl \rangle^{1/2} \langle n'l' | n'l' \rangle^{1/2}} \right] = \sum_{n'} \lambda_{nl, n'l'} \frac{\int dr \phi_{n'l'}(r) \delta \phi_{nl}(r)}{\langle nl | nl \rangle^{1/2} \langle n'l' | n'l' \rangle^{1/2}}. \quad (\text{C9})$$

The variational principle requires that the variation δK be stationary with respect to $\delta \phi_{nl}(r)$. Collecting Eqs. (C3)–(C9), we obtain the Hartree-Fock equations [Eq. (13)] where

$$Y_i(r) = \sum_{j,k} \frac{(1 + \delta_{n_i l_i, n_j l_j}) a_{n_i l_i, n_j l_j, k} Y^k(n_j l_j, n_j l_j, r)}{w_i \langle n_j l_j | n_j l_j \rangle}, \quad (\text{C10})$$

$$X_i(r) = \sum_{j \neq i, k} \frac{b_{n_i l_i, n_j l_j, k} Y^k(n_i l_i, n_j l_j, r) \phi_{n_j l_j}(r)}{w_i \langle n_j l_j | n_j l_j \rangle}, \quad (\text{C11})$$

and

$$\varepsilon_{ii} = \frac{2}{w_i} \left[\tilde{E}(n_i l_i) - \sum_k \frac{a_{n_i l_i, n_i l_i, k} F^k(n_i l_i, n_i l_i)}{\langle n_i l_i | n_i l_i \rangle^2} \right], \quad (\text{C12})$$

$$\varepsilon_{ij} = \frac{\lambda_{n_i l_i, n_j l_j} \langle n_i l_i | n_i l_i \rangle^{1/2}}{w_i \langle n_j l_j | n_j l_j \rangle^{1/2}}. \quad (\text{C13})$$

- [1] W. Kohn and L. J. Sham, *Phys. Rev.* **140**, A1133 (1965).
- [2] J. P. Perdew, K. Burke, and M. Ernzerhof, *Phys. Rev. Lett.* **77**, 3865 (1996).
- [3] M. Bühl, C. Reimann, D. A. Pantazis, T. Bredow, and F. Neese, *J. Chem. Theor. Comput.* **4**, 1449 (2008).
- [4] J. P. Perdew, *Int. J. Quantum Chem.* **28**, 497 (1985).
- [5] C. Adamo and V. Barone, *J. Chem. Phys.* **110**, 6158 (1998).
- [6] J. Muscat, A. Wander, and N. M. Harrison, *Chem. Phys. Lett.* **342**, 397 (2001).
- [7] J. Heyd, J. E. Peralta, G. E. Scuseria, and R. L. Martin, *J. Chem. Phys.* **123**, 174101 (2005).
- [8] A. M. Rappe, K. M. Rabe, E. Kaxiras, and J. D. Joannopoulos, *Phys. Rev. B* **41**, 1227(R) (1990).
- [9] N. J. Ramer and A. M. Rappe, *Phys. Rev. B* **59**, 12471 (1999).
- [10] J. P. Perdew and K. Schmidt, *Density Functional Theory and its Application to Materials*, edited by V. Van Doren, C. Van Alsenoy, and P. Geerlings, AIP Conf. Proc. No. 577 (AIP, New York, 2001), pp. 1–20.
- [11] M. Fuchs, M. Bockstedte, E. Pehlke, and M. Scheffler, *Phys. Rev. B* **57**, 2134 (1998).
- [12] J. R. Trail and R. J. Needs, *J. Chem. Phys.* **122**, 014112 (2005).
- [13] W. A. Al-Saidi, E. J. Walter, and A. M. Rappe, *Phys. Rev. B* **77**, 075112 (2008).
- [14] C. W. Greeff and W. A. Lester, *J. Chem. Phys.* **109**, 1607 (1998).
- [15] I. Ovcharenko, A. Aspuru-Guzik, and W. A. Lester, Jr., *J. Chem. Phys.* **114**, 7790 (2001).
- [16] X. F. Wu, E. J. Walter, A. M. Rappe, R. Car, and A. Selloni, *Phys. Rev. B* **80**, 115201 (2009).
- [17] <http://opium.sourceforge.net>.
- [18] C. Froese Fischer, *Comput. Phys. Commun.* **43**, 355 (1987).
- [19] J. C. Slater, *Quantum Theory of Atomic Structure* (McGraw-Hill, New York, 1960).
- [20] C. F. Fischer, *The Hartree-Fock method for Atoms: A Numerical Approach* (Wiley-Interscience, New York, 1977).
- [21] J. P. Perdew, M. Ernzerhof, and K. Burke, *J. Chem. Phys.* **105**, 9982 (1996).
- [22] P. Giannozzi, S. Baroni, N. Bonini, M. Calandra, R. Car, C. Cavazzoni, D. Ceresoli, G. L. Chiarotti, M. Cococcioni, I. Dabo, A. D. Corso, S. de Gironcoli, S. Fabris, G. Fratesi, R. Gebauer, U. Gerstmann, C. Gougoussis, A. Kokalj, M. Lazzeri, L. Martin-Samos, N. Marzari, F. Mauri, R. Mazzarello, S. Paolini, A. Pasquarello, L. Paulatto, C. Sbraccia, S. Scandolo, G. Sclauzero, A. P. Seitsonen, A. Smogunov, P. Umari, and R. M. Wentzcovitch, *J. Phys.: Condens. Matter* **21**, 395502 (2009).
- [23] V. Blum, R. Gehrke, F. Hanke, P. Havu, V. Havu, X. Ren, K. Reuter, and M. Scheffler, *Comput. Phys. Commun.* **180**, 2175 (2009).
- [24] A. D. Becke, *J. Chem. Phys.* **109**, 2092 (1998).
- [25] M. Ernzerhof and E. Scuseria, *J. Chem. Phys.* **110**, 5029 (1999).
- [26] Y.-i. Matsushita, K. Nakamura, and A. Oshiyama, *Phys. Rev. B* **84**, 075205 (2011).
- [27] G. Zhang and C. B. Musgrave, *J. Phys. Chem. A* **111**, 1554 (2007).
- [28] NIST Standard Reference Database Number 101, NIST Computational Chemistry Comparison and Benchmark Database, <http://cccbdb.nist.gov/> (2016).
- [29] H.-R. Liu, H. Xiang, and X. G. Gong, *J. Chem. Phys.* **135**, 214702 (2011).
- [30] P. Trucano and R. Chen, *Nature (London)* **258**, 136 (1975).
- [31] J. Toulouse, W. Zhu, J. G. Angyán, and A. Savin, *Phys. Rev. A* **82**, 032502 (2010).
- [32] D. R. Hamann, M. Schlüter, and C. Chiang, *Phys. Rev. Lett.* **43**, 1494 (1979).
- [33] L. Kleinman and D. M. Bylander, *Phys. Rev. Lett.* **48**, 1425 (1982).